Environmental Science Nano

Nanoparticle-Induced Structural Changes in Lung Surfactant Membranes: An X-ray Scattering Study

Journal:	*Environmental Science: Nano*
Manuscript ID	EN-ART-02-2018-000189.R2
Article Type:	Paper
Date Submitted by the Author:	09-Apr-2018

Complete List of Authors:	Behyan, Shirin; Concordia University, Chemistry and Biochemistry; Université de Montréal Borozenko, Olga; Université de Montréal; Concordia University, Chemistry and Biochemistry Khan, Abdullah; Concordia University, Chemistry and Biochemistry Faral, Manon; Université de Montréal Badia, Antonella; Université de Montréal DeWolf, Christine; Concordia University, Chemistry and Biochemistry

Environmental Significance Statement

Nanoparticle-Induced Structural Changes in Lung Surfactant Membranes: An X-ray Scattering Study

Shirin Behyan,[a,b] Olga Borozenko,[a,b] Abdullah Khan,[a] Manon Faral,[b] Antonella Badia,*[b,c] and Christine DeWolf*[a,c]

[a]Department of Chemistry and Biochemistry and Centre for NanoScience Research, Concordia University, 7141 Sherbrooke St. West, Montréal, QC H4B 1R6, Canada. E-mail: christine.dewolf@concordia.ca

[b]Address here. Département de chimie, Université de Montréal, C.P. 6128 succursale Centre-ville, Montréal, QC H3C 3J7, Canada. E-mail: antonella.badia@umontreal.ca

[c]FRQNT Quebec Centre for Advanced Materials.

*Corresponding Authors Contact Information:

E-mail: christine.dewolf@concordia.ca

E-mail: antonella.badia@umontreal.ca

The inhalation of ultrafine particulate, including engineered nanoparticles, can lead to respiratory health problems as these particles are inhaled without resistance and deposit in the alveolar region of the lung, where they are retained and interact with the lung surfactant membrane.Although much of the lung surfactant literature focuses on anionic nanoparticles, we find that cationic nanoparticles have a much greater impact on membrane structure and moreover, this impact occurs at much lower concentrations than previously considered. These structural changes have implications for the film mechanical properties that govern the breathing process, with the potential for immediate impairment of respiratory function.. These findings contribute to a better understanding of the biophysical impact of nanoparticle-lung surfactant interactions.

Environmental Science: Nano

ARTICLE

Nanoparticle-Induced Structural Changes in Lung Surfactant Membranes: An X-ray Scattering Study

Received 00th January 20xx,
Accepted 00th January 20xx

DOI: 10.1039/x0xx00000x

www.rsc.org/

Shirin Behyan,[a,b] Olga Borozenko,[a,b] Abdullah Khan,[a] Manon Faral,[b] Antonella Badia,*[b,c] and Christine DeWolf*[a,c]

The effect of low concentration (0.001 wt%) of charged silica nanoparticles (NPs) on the molecular structure of lung surfactant monolayers was investigated at the air/water interface using grazing incidence X-ray diffraction (GIXD) and X-ray reflectivity (XR). The lipid systems investigated included 1,2-dipalmitoyl-sn-glycero-3-phosphocholine (DPPC), mixtures of DPPC and 1,2-dilauroyl-sn-glycero-3-phosphocholine (DLPC) or 1-palmitoyl-2-oleoyl-sn-glycero-3-phosphoglycerol (POPG), and Infasurf (a clinical lung surfactant formulation). In all cases, the anionic silica NPs interacted with the films but induced only small structural changes. By contrast, the cationic NPs induced a significant reduction of the alkyl chain tilt angle when anionic lipid was present. This appears to be associated with a condensation of the POPG lipids that would alter the ratio of liquid-expanded and condensed phases. Thus, this study reveals that low concentrations of cationic NPs can induce structural changes that could impact film mechanical properties that are important for pulmonary function.

Introduction

We investigated the immediate and direct impact of aqueous dispersions of anionic and cationic silica nanoparticles (NPs) on the structure of Langmuir monolayers of lung surfactant and relevant lipid-only mixtures at the air/water interface. Detailed information regarding two-dimensional order on the angstrom scale was obtained using synchrotron grazing incidence X-ray diffraction (GIXD) and X-ray reflectivity (XR) techniques.[1,2] GIXD is sensitive to the ordered condensed phase of the monolayer, while XR is sensitive to both the disordered (liquid-expanded) and ordered phases. The combination of these two techniques provides a more complete picture of the monolayer structure and nanoparticle-induced effects.

NPs can enter into the human body via inhalation, skin penetration, ingestion, or direct injection into the bloodstream in medical applications.[3,4] Among these different entry routes, the respiratory tract, with its large surface area, facilitates the entry of airborne NPs to the lung through inhalation.[5] After inhalation, these particles can be deposited into the alveolar region of the lung,[6] where they are retained and likely interact with (and/or are embedded into) the lung surfactant monolayer.[7,8] This lipid-protein monolayer film coats the alveolar air/fluid interface of the lungs and the reversible compression of this film during inhalation and exhalation via a monolayer-multilayer equilibrium reduces the work of breathing and prevents alveolar collapse. The physicochemical interaction of NPs with this pulmonary surfactant film can lead to its malfunction or even inactivation.[9]

The growing demand for applications of nanomaterials has urged many research groups to study the impact of various kinds of NPs on the lungs. These studies generally fall under three main directions: toxicology studies which focus on the link between inhaled NPs and pulmonary disease, including the consequential cell response after exposure,[10–12] studies which look at the effect of NPs on lung surfactant function,[13–15] and studies that focus on structural and morphological effects.[16–21] These aforementioned effects of NPs depend on the surface properties, shape, solubility, surface charge, and size of the NPs.[16,22]

Hydrophobic NPs have a much higher probability of embedding within the hydrophobic alkyl chain region of lipid layers and it has been shown that these are retained in the lung surfactant film even with repeated compression-expansion cycles.[17,23] Such highly surface-active hydrophobic NPs have been shown to alter lung surfactant film morphology and domain structure,[9,18–20] induce fluidization and/or expansion of the condensed domains,[18,20] and embed preferentially in the fluid phase[17] or at phase boundaries[20]. Many of these effects are dose-, time-, and size-dependent.[13–15,18,20,24] Hydrophilic particles are less likely to remain embedded in the hydrophobic surface film, unless coated by the lipid to produce a hydrophobic coating.[25] For hydrophilic particles that reside in the aqueous subphase, a key parameter

[a] Department of Chemistry and Biochemistry and Centre for NanoScience Research, Concordia University, 7141 Sherbrooke St. West, Montréal, QC H4B 1R6, Canada. E-mail: christine.dewolf@concordia.ca
[b] Département de chimie, Université de Montréal, C.P. 6128 succursale Centre-ville, Montréal, QC H3C 3J7, Canada. E-mail: antonella.badia@umontreal.ca
[c] FRQNT Quebec Centre for Advanced Materials.

†Electronic Supplementary Information (ESI) available: Surface pressure-area isotherms of POPG on subphases of water and cationic silica NPs, XR fits, maxima of Bragg peak and Bragg rod fits of the GIXD measurements, and physical characteristics of the silica NPs. See DOI: 10.1039/x0xx00000x

governing their interaction with the lung surfactant film is the surface charge. Again, these particles have been shown to interact with the lipid domain boundaries while decreasing the line tension in these areas,[4] increase the film fluidity,[25] and hinder domain formation.[25,26] Molecular arrangement changes have been inferred from morphological studies, but have not been shown via direct measurements of the phase structure.[25]

To date, studies on the NP-induced dysfunction of lung surfactant have mainly focused on relatively high concentrations of NPs. For systems in which the NPs are co-spread with the lipid, the ratio of NP/lipid ranges from 0.001 to 3 mg NPs/mg lipid. For NPs dispersed in the aqueous subphase, in particular for silica NPs, frequently concentrations in the range of 1 wt% are used.[25–27] One study reported that at low concentrations (10^{-5} and 10^{-4} g/L NPs in the subphase) no impact of negatively-charged, polystyrene beads was observed.[28] We chose 0.001 wt% as it was the lowest concentration for which any of the systems investigated here showed an impact on the surface-pressure area isotherms.

The NP types chosen for this study are ion-stabilized cationic and anionic amorphous silica particles of approximately 20 nm diameter (see Table S1 of ESI† for the NP characteristics). Contrary to hydrophobic NPs that are prone to aggregation and also likely to be retained in the film at the air/water interface, the hydrophilic silica nanoparticles are easily dispersed in water and most likely to pass through the film into the lung lining fluid. An aqueous dispersion of NPs under the Langmuir monolayer allows one to study the particle association with and impact on lung surfactant films. Moreover, given the presence of charged lipids and proteins in lung surfactant,[29] charged NPs are of particular interest given the potential for strong electrostatic interactions. Silica NPs are widely used as fillers, binders, and catalysts. Furthermore, silicon has been found to be a frequent component of atmospheric nanoparticles.[30] Inhaled amorphous silica particles are believed to produce an inflammatory pulmonary condition in rats[31] and silicosis, an occupational pulmonary disease caused by the inhalation of crystalline silica dust.[32]

Infasurf, a solvent extract of calf lung lavage, was used as a natural lung surfactant and is comprised mainly of 91 wt% phospholipids (including 43% DPPC and 4.5% phospatidylglycerol, PG), 5-8 wt% cholesterol, and 1.6-2.2 wt% of the hydrophobic proteins SP-B and SP-C.[29] Lipid-only monolayers were used to mimic the major phospholipid constituents of lung surfactant and to discern the impact of surface-specific proteins on the interaction of NPs with lung surfactant. The systems selected represent (i) the condensed phase of lung surfactant (1,2-dipalmitoyl-sn-glycero-3-phosphocholine, DPPC), (ii) the saturated:unsaturated lipid balance of lung surfactant and charge difference between the condensed and fluid phases (DPPC and 1-palmitoyl-2-oleoyl-sn-glycero-3-phosphoglycerol, POPG, in 7:3 mole ratio). An analogous binary mixture that comprises a similar condensed: fluid phase balance but with only zwitterionic headgroups, i.e. no charge difference between the phases (DPPC and 1,2-dilauroyl-sn-glycero-3-phosphocholine, DLPC, in a 7:3 mole ratio) was also investigated (see Scheme 1).

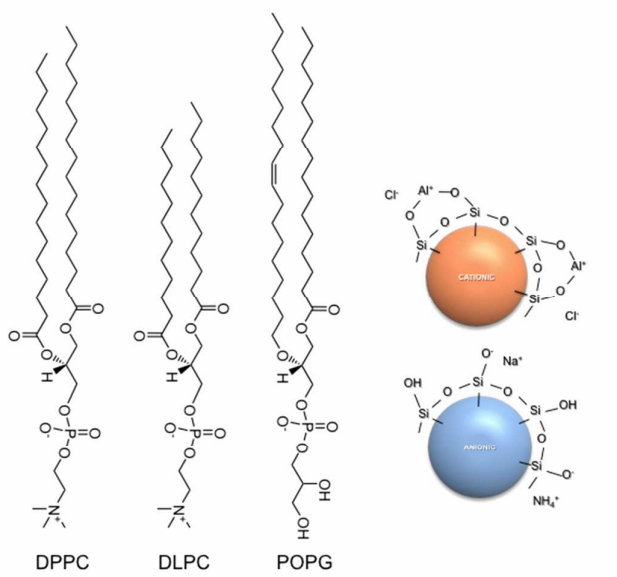

Scheme 1. Molecular structures of DPPC, DLPC, and POPG (left), and cationic and anionic silica nanoparticles (right).

This study uses both GIXD and XR to systematically probe the structural effects of charged silica NPs on lung surfactant monolayers. We investigate the impact of the NPs on the structure of the monolayers at high lateral surface pressure (35 mN/m) to ensure that the monolayers are laterally phase-separated into the condensed and liquid-expanded phases and still be below the squeeze-out plateau of Infasurf. We show that the nature of the liquid-expanded phase and the NP surface charge influence the unit cell packing of the condensed phase. Furthermore, we show that in the binary DPPC:POPG mixture and Infasurf, the cationic silica NPs not only change the molecular ordering of the condensed phase, they also cause the condensation of the POPG-enriched fluid phase, which additionally leads to a very small tilt angle of the alkyl chains for the DPPC-rich condensed phase that has not previously been observed at a similar temperature and pressure.[33,34]

Materials and Methods

Materials

1,2-dipalmitoyl-sn-glycero-3-phosphocholine (DPPC), 1-palmitoyl-2-oleoyl-sn-glycero-3-phosphoglycerol (POPG) and 1,2-dilauroyl-sn-glycero-3-phosphocholine (DLPC) were purchased as dry powders form Avanti Polar Lipids (purity >99%) and used without further purification. The main phase transition temperatures (Tm) of the lipids are: DPPC 41 °C, DLPC -2 °C, and POPG -2 °C.[35] Infasurf was donated by ONY, Inc. (Amherst, NY). Ultrapure deionized water with resistivity of 18.2 MΩcm was obtained by the purification of distilled water with an Easypure II LF or Milli-Q gradient purification system. The colloidal silica Levasil 200S (cationic) and Bindzil

30/360 (anionic) were donated by Akzo Nobel and received as aqueous dispersions (30% by weight). Ruby muscovite mica sheets (V-1/V-2, optical grade 1) were obtained from S&J Trading Inc. (Queens, NY).

Surface Pressure-Area Isotherms

Lipid solutions with a total lipid concentration of 1 mM were prepared for DPPC, DPPC:DLPC, and DPPC:POPG and 1 mg/mL for Infasurf. A molar ratio of 7:3 was used for the DPPC:DLPC and DPPC:POPG mixtures. A 9:1 v/v mixture of heptane/ethanol was used as a solvent to prepare the DPPC:DLPC solution, while spectrograde chloroform was used as the solvent for the other lipid systems. The Infasurf suspension was first lyophilized and then mixed with chloroform to obtain the desired solution. The aqueous dispersions containing 0.001 wt% of Levasil or Bindzil NPs used as the subphases in the Langmuir trough were prepared by a 3.3×10^5-fold dilution of the colloidal silica concentrates with ultrapure water. DPPC (90 μL), DPPC:POPG (90 μL), DPPC:DLPC (90 μL), and Infasurf (100 μL) were spread on the surface (area of 705 cm^2) of the aqueous subphase (volume of 375 mL) of a 702 BAM Langmuir trough (Nima Technology Ltd., Coventry, England) thermostatted at 22.0 ± 0.5 °C. After solvent evaporation (20 min), the lipid monolayer was symmetrically compressed at a rate of 8 cm^2/min (or 1.5 $Å^2$/(molecule.min)). The surface pressure was measured with a precision of 0.1 mN/m using a Wilhelmy balance and a roughened platinum plate. For each phospholipid system, surface pressure-area isotherms were repeated until three overlapping isotherms were obtained on pure water and with NPs. Between measurements on ultrapure water or with a given NP type, the Langmuir-Blodgett trough was cleaned thrice with ethanol (95%). Between NP types, the trough was cleaned with dishwashing detergent.

Langmuir Monolayer Transfer onto Mica

Monolayer films of DPPC, DPPC:POPG, DPPC:DLPC, and Infasurf were transferred from the air/water interface (area of 768 cm^2) of a KSV 3000 trough (KSV Instruments Ltd., Helsinki, Finland) onto freshly-cleaved mica. The inverse (horizontal) Langmuir-Schaefer technique described by J.A. Zasadzinski et al.[36] was used to deposit the DPPC:POPG, DPPC:DLPC and DPPC films. To hold the substrate, a custom-made, stainless steel transfer unit was used. First, the unit with the immobilized mica was submerged in the aqueous subphase < 1 mm below the water surface. Then, the phospholipid solution was spread at the air/water interface. After solvent evaporation (20 min), the monolayer was symmetrically compressed to 35 mN/m at 15 cm^2/min or 2.5 $Å^2$/(molecule.min). The DPPC:POPG and DPPC:DLPC films were transferred onto the substrate right after the target pressure was reached. DPPC was held at 35 mN/m for 20 min before horizontal deposition. The compression barriers were stopped and the subphase carefully aspirated out of the trough using a Pasteur pipet to lower the subphase level below the top of the transfer unit so that the lipid head groups of the floating monolayer contacted the underlying mica. The knife-edge rim of the transfer unit cut through and held the monolayer at a fixed molecular area and surface pressure. The Langmuir-Blodgett technique was used to deposit the Infasurf monolayer onto the mica. The mica substrate was submerged vertically into the water subphase and the Infasurf monolayer formed. The monolayer was compressed to and held for 20 min at a target pressure of 35 mN/m. The substrate was then vertically withdrawn (upstroke) from the water subphase at a rate of 5 mm/min. The solid-supported films were allowed to dry under ambient conditions for 30 min and imaged by AFM within 24 h of their preparation.

Atomic Force Microscopy (AFM)

AFM imaging was performed in air on a Dimension ICON AFM (Bruker, Santa Barbara, CA) in ScanAsyst mode using silicon nitride probes with nominal spring constant of 42 N/m, resonance frequency of 300 kHz, and tip radius of <10 nm. Images were recorded at a scan rate of 1 Hz, 512 × 512 pixel resolution, and analyzed with Nanoscope software version 7.30.

Zeta Potential and Dynamic Light Scattering

The surface charge of the anionic and cationic NPs (0.001 wt% dispersions) and the hydrodynamic radius of the particles were measured using a zeta potential analyzer (Malvern ZETASIZER NANO) and dynamic light scattering (DLS). All tubes and plastic cuvettes were dried with a flow of nitrogen gas before the addition of the NP suspensions. Approximately 600 μL and 700 μL of the NP suspension were added to the plastic cuvettes used for DLS and zeta potential measurements, respectively. The refractive index of the dispersant (water) was set to 1.33 and the refractive index of the silica NPs was set to 1.46. The experiments were performed at a temperature of 22.0 ± 0.5 °C.

Grazing Incidence X-ray Diffraction (GIXD)

The GIXD experiments were performed at beamline 15-ID-C ChemMatCARS at the Advanced Photon Source (APS) in Argonne National Laboratory with the following parameters: X-ray beam wavelength of 1.239 Å, incidence angle of 0.0906°, horizontal size of 20 μm, and vertical size of 120 μm, leading to a beam footprint of 20 μm by 7.6 cm. The detector used was the 2D Swiss Light source PILATUS 100K set to single-photon counting mode. Two sets of slits, one placed in front of the detector and the other placed 292.0 nm from the sample, were used to minimize intense low-angle scattering. Experiments were performed at the air/water interface of a 340 cm^2 Langmuir trough, where the monolayer was spread and then compressed at a speed of 5 cm^2/min (equivalent to 1.5 $Å^2$/(molecule.min)) using a mobile barrier after 20 min of equilibration time.

The measured GIXD data is plotted as contour plots of the intensity as a function of both the horizontal (q_{xy}) and the vertical (q_z) scattering vector components. The lattice spacing d_{hk} was obtained from the in-plane diffraction data as d_{hk} =

$2\pi/q_{xy}^{hk}$, where the Miller indices h, k were used to index the Bragg peaks needed to calculate the unit cell parameters for the in-plane lattice. The full width at half maximum (fwhm) of the Bragg peaks after correction for the instrumental resolution (0.0084 Å^{-1}) was used to calculate the in-plane correlation length using the Scherrer formula[37] as:
$\xi_{xy} \approx 0.9 \times 2\pi/fwhm_{intrinsic}(q_{xy})$ where,
$fwhm_{intrinsic}(q_{xy}) = \left[fwhm_{intrinsic}(q_{xy})^2 - fwhm_{resolution}(q_{xy})^2\right]^{1/2}$.
The fwhm of the Bragg rods was used to estimate the vertical correlation length as:
$L \approx 0.9 \times 2\pi/fwhm(q_z)$.[38] All GIXD experiments were performed at a lateral surface pressure of 35 mN/m and temperature of 22.0 ± 0.5 °C.

X-ray Reflectivity (XR)

XR is measured as a function of the vertical scattering vector component (q_z). XR probes the electron density variation $\rho(z)$ of the vertical structure of the layers at the air/water interface. A slab model was used to represent the monolayer as a stack of slabs, with each slab having a constant thickness and electron density. The electron density profile $\rho(z)$ was laterally averaged over both the ordered and disordered parts of the monolayer under the footprint of the X-ray beam and was calculated by a sum of error functions as:

$$\rho(z) = \frac{1}{2}\sum_{i-0}^{N-1} \mathrm{erf}\left(\frac{z-z_i}{\sqrt{2}\sigma}\right)(\rho_{i+1} - \rho_i) + \frac{\rho_0+\rho_N}{2}$$

where, $\mathrm{erf}(z) = \left(2/\sqrt{\pi}\right)\int_0^z e^{-t^2}\,dt$, N is the number of internal interfaces, σ is the surface roughness which is calculated from capillary wave theory, z_i is the position of the ith interface, ρ_i is the electron density of the ith interface, and ρ_0 is the electron density of the aqueous subphase.[39,40] X-ray reflectivity data was analyzed using an open source software developed by Wei Bu, beamline scientist at ChemMatCARS. The measured X-ray reflectivity $R(q_z)$ is normalized by the Fresnel reflectivity $R_F(q_z)$ which, is calculated for a sharp air/water interface. X-ray reflectivity was calculated using the Parratt method.[41–44] Nonlinear least-squares fitting was used to determine the minimum number (N-1) of internal slabs to best fit the X-ray reflectivity data. In our XR data analysis, all systems were treated as a homogeneous monolayer film although lateral phase separation occurs under the experimental conditions. This assumption was made based on the sizes of the condensed and liquid-expanded phases which are less than the footprint of the X-ray beam in all of our systems. This assumption has been previously used in the literature, where the domain sizes of the phase-separated patches are smaller than the X-ray beam footprint.[45] All XR experiments were performed at a lateral surface pressure of 35 mN/m and temperature of 22.0 ± 0.5 °C.

Results and Discussion

Phase Behavior and Structure of the Different Lipid Systems on Water

Surface Pressure-Area Isotherms. The surface pressure-area isotherms for the four systems, DPPC, DPPC:DLPC (7:3), DPPC:POPG (7:3), and Infasurf, on ultrapure water at 22 °C are shown in Figure 1. Although 22 °C is not physiological temperature, literature has shown the phase behaviour of DPPC, DPPC:POPG and Survanta (a bovine lung solvent extract) to be similar but with the phase transitions shifted to higher surface pressures.[46] It should be noted that the isotherm for Infasurf is reported in terms of the trough area and not molecular area since its exact composition is not known. The isotherms resemble those reported in the literature.[29,47,48] The single-component DPPC film undergoes a liquid-expanded (LE)-to-condensed (C) phase transition as evidenced by the LE-C plateau between 8 and 10 mN/m. In the case of the binary lipid mixtures, the phase transition is broadened and shifted to higher surface pressures between 15 and 20 mN/m. The unsaturated POPG and shorter-chain, disaturated DLPC both remain in the LE phase until their respective collapse pressures,[47,49] as confirmed by the lack of diffraction peaks in GIXD (data not shown). In binary mixtures with DPPC, this leads to lateral phase separation into DPPC-rich condensed domains within a DLPC- or POPG-rich fluid or LE phase. In the case of the more complex Infasurf mixture, the LE-C phase transition is no longer apparent in the isotherm. The plateau at 40 mN/m is associated with squeeze-out of the LE phase and reservoir formation.[50,51] After the squeeze-out, the surface pressure increases again due to compression of the residual condensed phase. The DPPC, DPPC:POPG and Infasurf monolayers can be compressed to high surface pressures and finally collapse between 67 and 70

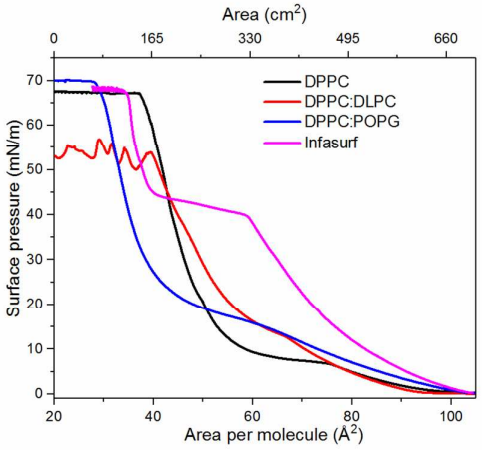

Figure 1. Surface pressure-area isotherms of DPPC, DPPC:DLPC (7:3), DPPC:POPG (7:3), and Infasurf on a pure water subphase at 22.0 ± 0.5 °C. Isotherms of DPPC, DPPC:DLPC, DPPC:POPG are reported in terms of molecular area (bottom axis). The isotherm of Infasurf is presented in terms of the trough area (top axis).

mN/m, while the DPPC:DLPC monolayer collapses at the lower collapse pressure of DLPC (53 mN/m), as has been previously reported.[52]

AFM Images and X-ray Scattering Results. The lipid monolayers were all transferred onto mica at 35 mN/m by inverse Langmuir-Schaefer[36] to limit the transfer-induced

distortion of the film morphology and phase structure imaged by atomic force microscopy (AFM). The AFM images of the transferred films are given in Figure 2 and the tabulated analyses are presented in Table 1. The GIXD contour plots of the monolayers at the air/water interface acquired at 35 mN/m are shown in Figure 3. The fitted unit cells parameters are given in Table 2 and the fitted peak positions can be found in ESI†. The XR data is presented in Table 3.

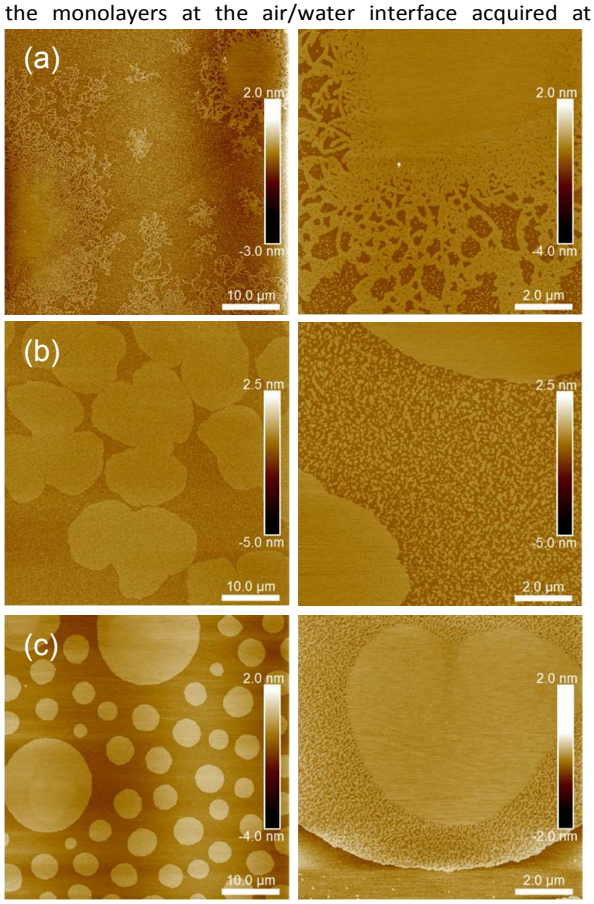

Figure 2. AFM height images of the lipid monolayers deposited onto mica: (a) DPPC:DLPC (7:3), (b) DPPC:POPG (7:3), and (c) Infasurf. The monolayers were transferred by inverse Langmuir-Schaefer at 35 mN/m (a, b) or by Langmuir-Blodgett at 33 mN/m (c). Left-hand side images are 50 × 50 µm^2 and right-hand side images are 10 × 10 µm^2.

The single-component DPPC monolayer presents a homogeneous condensed phase (AFM data not shown). The diffraction pattern shows three low-order reflections (10, 01, $1\bar{1}$) with their Bragg rod maxima above the horizon ($Q_z > 0$), characteristic of a system with an oblique chain lattice and tilt azimuth in the non-symmetry direction (between nearest neighbor (NN) and next nearest neighbor (NNN)).[2] d spacings of 4.60 (10), 4.47 (01), and 4.28 ($1\bar{1}$) Å were calculated from fits of the Bragg peaks and a chain tilt angle of 27.1° was determined from the Bragg rod analysis. The large tilt angle of the DPPC chains is comparable to the values reported in the literature[33] at similar surface pressures and temperatures and has been ascribed to the area mismatch of the hydrated phosphatidylcholine head group (50 Å^2)[53] and the alkyl chains (38 Å^2)[53,34]. This area mismatch is compensated by tilting the chains until a balance between the projected area of the chains and that of the head group can be achieved.[34]

The DPPC:DLPC, DPPC:POPG, and Infasurf monolayers show two phases of different thicknesses in AFM (Figure 2). The proportion of the films occupied by the thicker condensed phase ranges from 40 % to 65 % (Table 1), with DPPC:POPG showing the greatest coverage of condensed phase. The height difference between the LE and C phases is very similar for all three systems and ranges from 5 to 6 Å. One should note that the height difference obtained by AFM is strongly dependent on the force applied to the sample during imaging.[54]

DPPC and DLPC have previously been reported to exhibit phase separation with partial miscibility in monolayers.[52] The AFM image of DPPC:DLPC (Figure 2(a)) confirms the presence of lateral phase separation. As previously reported, at higher pressures, the condensed phase breaks up to form branch-like extensions that protrude from a circular nucleus.[52] A similar effect has been reported for giant unilamellar vesicles and attributed to partial lipid miscibility due to a low chain mismatch (four methylenes).[47] The mixed monolayer exhibits an oblique lattice with tilt azimuth in the non-symmetry direction (Figure 3), analogous to pure DPPC. However, the diffraction peaks are of significantly lower intensity, which may be due to phase separation, i.e., the reduced amount of condensed phase in the beam footprint, and/or a lower crystallinity of the condensed phase due to the break up of the condensed phase domains when the system is held at constant high pressure. d spacings of 4.65, 4.59, 4.29 Å and a hydrocarbon chain tilt of 28.4° were calculated for the mixed monolayer on the water subphase. In comparison to pure DPPC, the unit cell shows an expansion and the chains are more tilted away from the surface normal, with a correspondingly larger projected area per chain (see Table 2), resulting from an increased area mismatch between the shorter-chain DLPC and longer-chain DPPC. The incorporation of DLPC in the DPPC condensed phase is confirmed by the shifts in the diffraction peak positions as well as the shorter vertical coherence length (13.5 Å from GIXD) and smaller average alkyl chain thickness (13.3 Å from XR) compared to those of DPPC (16.5 Å and 15.9 Å, respectively). Because the GIXD measurements are only sensitive to the ordered phase of the film, we observe a higher value for the alkyl chain region thickness in comparison to the XR value that is an average value for the alkyl chain region of the entire (non-homogeneous) film, that is, the average thickness of both the condensed and fluid phases.

The DPPC:POPG monolayer film exhibits compact micron-size lobe-shaped domains; smaller submicron-size condensed phase domains are also found in the fluid phase (Figure 2(b)). The GIXD diffraction pattern again shows three diffraction peaks and an oblique unit cell in agreement with the literature.[34] However a lower alkyl chain tilt angle of 20.0° was calculated for this system. It has been shown that POPG partially incorporates into the molecular packing structure of the condensed DPPC phase.[34] Replacing the bulkier phosphatidylcholine head group with phosphatidylglycerol reduces the area mismatch between the head groups and

chains, leading to a smaller tilt angle.[34] Unlike DPPC:DLPC, the diffracted intensity is not as dramatically decreased for the DPPC:POPG system despite the monolayer being phase separated. This is in agreement with the greater proportion of condensed phase in the film (Table 1). The incorporation of POPG into the DPPC crystalline phase causes the average in-plane correlation length (ξ) to increase from 151.6 Å in pure DPPC to 166.1 Å in DPPC:POPG.

Two distinct size populations of condensed phase domains are observed for Infasurf (Figure 2(c)). The larger domains are approximately 15-20 μm in diameter while the smaller are 1-2 μm. There is no evidence of submicron condensed domains in

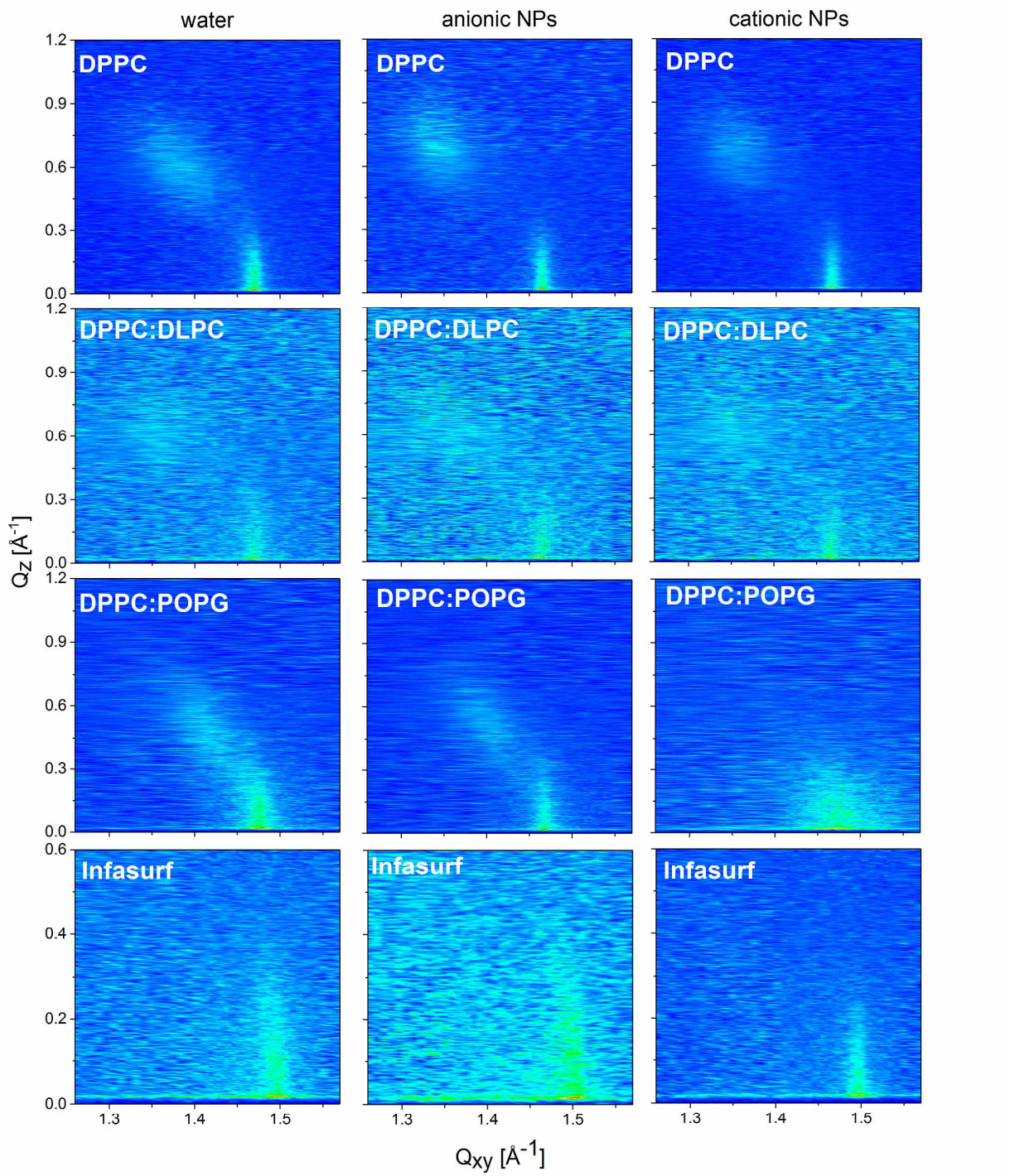

Figure 3. Contour plots of the X-ray intensities versus in-plane scattering vector components Q_{xy} and Q_z for DPPC, DPPC:DLPC (7:3), DPPC:POPG (7:3), and Infasurf on subphases of ultrapure water (left), 0.001 wt% anionic silica NPs (middle), and 0.001 wt% cationic silica NPs (right) at a surface pressure of 35 mN/m and temperature of 22.0 ± 0.5 °C.

the fluid phase. Moreover, the larger domains reveal a domain-in-domain structure that has previously been attributed to the formation of both a cholesterol-rich liquid-ordered and DPPC-rich tilted condensed phase.[29] The complex lipid composition, multiple phases present, and reduced alkyl chain tilt angle in Infasurf prevented an accurate determination of the diffracted peak positions. It is however clear that the diffraction peaks are found at lower Q_z values than the lipid-only systems, indicative of a smaller tilt angle. Previous literature reports indicate three diffraction peaks, an oblique alkyl chain lattice, and a low tilt angle of 6.9 ± 1°.[55]

Effect of the Silica Nanoparticles on the Structural Organization

This study compares the effects of cationic and anionic amorphous silica particles of approximately 20 nm diameter on the structure and phase behavior of lung surfactant films. Additional experiments were performed with neutral silica NPs, however these were not stable and acquired a negative charge with time (i.e., zeta potential measurements), and consequently showed a similar effect to that of the anionic silica NPs (data not shown). The lipids were spread on a NP containing subphase and subsequently compressed after 20 min of equilibration (see experimental section). Longer equilibration times were also investigated but showed no significant effect. We worked at a NP concentration of 0.001 wt% in the subphase (equivalent to 0.01 g/L) and a corresponding lipid to NP ratio of approximately 150:1. The surface pressure-area isotherms collected on the aqueous nanoparticle subphases showed no significant differences, with the exception of DPPC:POPG and Infasurf (Figure 4). In the case of DPPC:POPG, both particle types induce an expansion of the mixed monolayer but have no impact on the collapse pressure. By contrast, only the cationic NPs impact the Infasurf isotherm, but only at pressures above the squeeze-out plateau which begins at ~40 mN/m.

The results of the GIXD and XR measurements performed on monolayers formed on aqueous dispersions of the silica NPs are presented in Tables 2 and 3 and Figure 3. In all cases, fitting of the reflectivity curves required an additional layer in the presence of the NPs, confirming their presence at the aqueous/monolayer interface. Moreover, the anionic and cationic particles yielded layer thicknesses of 150-160 Å and 223-228 Å, respectively, in agreement with the average particle sizes determined by DLS (Table S1 of ESI†).

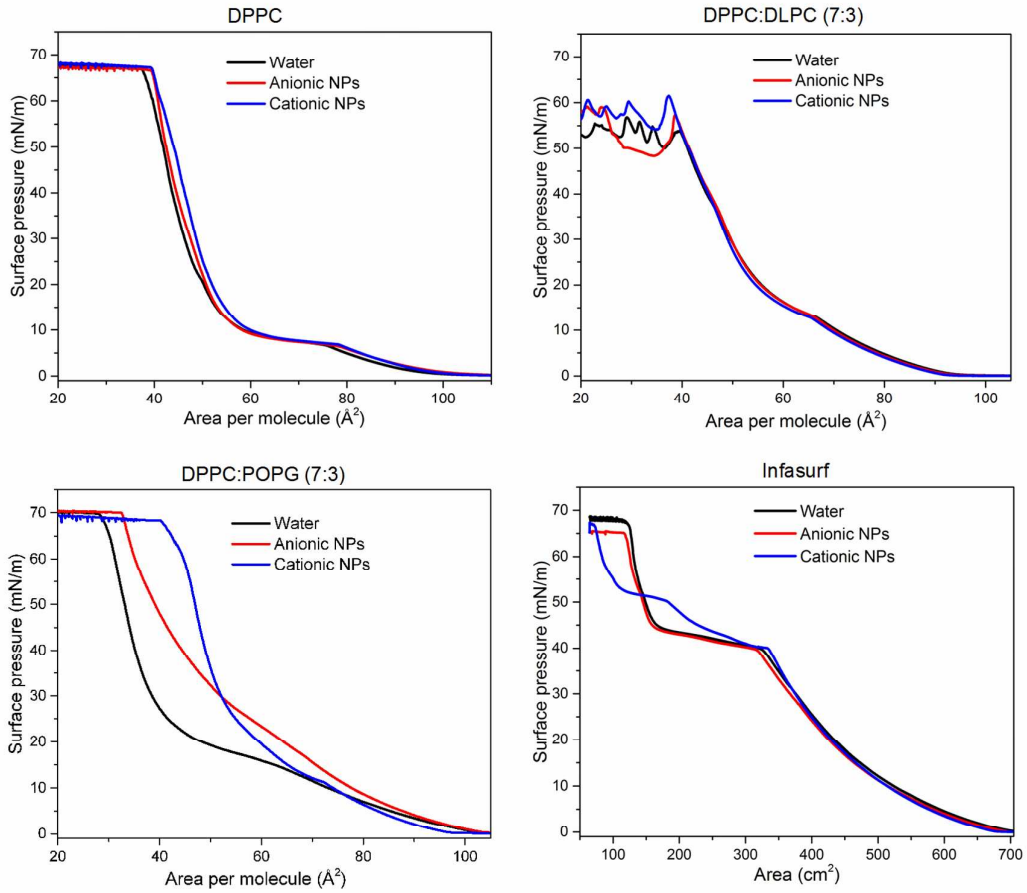

Figure 4. Surface pressure-area isotherms of DPPC, DPPC:DLPC (7:3), DPPC:POPG (7:3), and Infasurf on pure water versus aqueous subphases containing 0.001 wt% of anionic or cationic silica NPs at 22.0 ± 0.5 °C.

Anionic Silica NPs. For all four lipid systems on the anionic NP-containing subphase, the alkyl chains remain in an oblique unit cell with tilt between NN and NNN. Additionally, the particles only induce minor changes in the d-spacings and alkyl chain tilt angles that may simply be due to the reorientation of the head groups to interact with the charged particles. Both DPPC and DPPC:POPG exhibit a small expansion of the unit cell in the presence of the NPs. Although the diffraction peaks of Infasurf could not be definitively fitted, as already mentioned, the contour plots clearly indicate that the diffraction peak shifts to a higher value of Q_z, indicating a unit cell expansion similar to that of DPPC and DPPC:POPG. In the case of DPPC:POPG, this small difference can be surprising given that the NPs hinder the condensed phase formation, shifting the LE-to-C plateau to higher surface pressure (Figure 4). What this suggests is that the anionic NPs have an effect on the molecular spacing of the POPG-rich LE phase, which is not detectable by GIXD. By contrast, the changes in unit cell of the condensed phase of DPPC:DLPC shows a small contraction that may be a consequence of the expansion already induced by the DLPC. Additionally, the low intensity of the diffraction peaks makes an absolute determination of this change difficult.

The XR results show subtle changes in the alkyl chain thickness in all of the lipid systems compared to those on the water subphase, in agreement with the small changes in the chain tilt angles obtained from the diffraction data. The thickness of the head group region however shows a decrease consistent with a head group re-orientation. Such re-orientations have previously been demonstrated in the presence of charged amphiphiles and counterions.[56] It has been shown that in the water subphase, the head group is positioned with the phosphorous-nitrogen axis oriented approximately parallel to the water subphase.[56,57] In the presence of positively-charged entities, it adopts a new orientation with tilting of the nitrogen towards the water subphase. By contrast, in the presence of negatively-charged entities, the head group adopts a conformation with the nitrogen facing towards the monolayer film.[56] The latter re-orientations lead to a decrease in the thickness of the head group region, consistent with our XR results.

Cationic Silica NPs. The GIXD results of the DPPC and DPPC:DLPC systems show that the alkyl chains remain in an oblique unit cell with tilt between NN and NNN. Like the anionic NP subphase, a slight expansion of the unit cell is observed along with a small increase in the alkyl chain tilt and a commensurate decrease in the thickness of the alkyl chain region. The XR results also confirm the adsorption of the NPs to the monolayer film. However, in this system the thickness of the head group region is slightly increased relative to the water subphase. As discussed above, DPPC has been reported to re-orient in the presence of cationic entities and tilting of the nitrogen towards the subphase yields an increased head group thickness.

For DPPC:POPG, the cationic NPs induce a significant change in the diffraction pattern, which comprises two Bragg peaks, both with their Bragg rod maxima above the horizon ($Q_z > 0$), indicating a centered rectangular unit cell with the tilt azimuth in the NNN direction. From the fitted Bragg peaks, d spacings of 4.35 and 4.26 Å and a hydrocarbon tilt angle of 6.8° were calculated, indicating that the cationic NPs induce a significantly more compact and less tilted condensed phase. Such a small tilt angle has not been observed for the DPPC condensed phase at a similar temperature and pressure,[33,34] except in the presence of chaotropic agents,[58] i.e., pure DPPC monolayers on water do not achieve this low tilt angle. Given that the cationic NPs do not have a significant impact on pure DPPC, this must be a consequence of the anionic POPG that has some partial miscibility in the DPPC-rich condensed phase.
In order to probe this interaction, XR and GIXD measurements were performed on pure POPG films. As expected, no diffraction peaks were observed for POPG on either water or the subphase containing the anionic NPs (data not shown). However, in the presence of the cationic NPs, a weak diffraction peak is observed, indicating a local condensation of the POPG at 35 mN/m. The peak intensity increases with compression and a sharp peak was observed by 44 mN/m corresponding to a hexagonal lattice of untilted chains (Figure 5 and Table S3). Isotherms of POPG on a cationic NP subphase exhibit a change in compressibility (relative to those on water), commensurate with a more condensed monolayer (Figure S1).

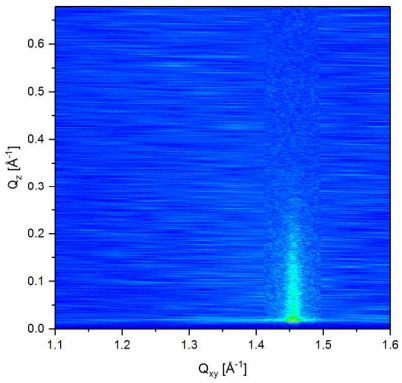

Figure 3. Contour plot of the X-ray intensity versus the in-plane scattering vector components Q_{xy} and Q_z for POPG on the subphase containing 0.001 wt% cationic NPs at a surface pressure of 44 mN/m and temperature of 22.0 ± 0.5 °C.

We cannot conclude whether the cationic NPs induce an additional condensation of the POPG molecules, which increases the proportion of POPG in the condensed phase and consequently reduces the tilt angle of this phase and/or whether the cationic NPs induce a strong re-orientation of the POPG already distributed throughout the condensed phase. Both a single condensed phase structure and overlapping diffraction peaks from two distinct condensed phases were fit to the data, however the single condensed phase gave a better fit considering the peak position of pure POPG on cationic NPs. Furthermore, with the very small tilt angle of 6.8° for DPPC:POPG, one expects an increase in the hydrocarbon chain region thickness. The vertical coherence length (15.0 ± 0.6 Å,

GIXD) as well as the chain region thickness (15.5 Å, XR) both show a decrease in the alkyl chain thickness (approximately 1.5–2.0 Å compared to water). A similar decrease is also observed for pure POPG (ESI†, Table S4). This suggests that the strength of the cationic NP-anionic lipid interactions pulls the monolayer film towards the aqueous subphase.

The contour plots for Infasurf, which contains a significant proportion of anionic lipids,[29] clearly indicate that the diffraction peak also shifts to a lower value of Q_z, indicating a tilt angle reduction. The extent of this reduction is lower than observed with DPPC:POPG, however it should be noted that the tilt angle is already quite small for Infasurf on water and the LE phase for Infasurf comprises both charged and uncharged lipids. Thus, the amount of POPG that can be condensed is lower.

Noteworthy is that the interaction of DPPC:POPG with the cationic nanoparticles induces a tilt angle similar to that of Infasurf on water based on the position of the out-of-plane scattering vector components (Q_z). This could imply that the positively-charged proteins (SP-B and SP-C) exert a condensing effect analogous to that of the cationic NPs. Hädicke and Blume[59] reported that cationic peptides can accumulate on negatively-charged lipids and serve to minimize charge repulsion, thereby inducing a film contraction. This condensing effect was reported for both the negatively-charged condensed and LE phases. Although cationic nanoparticle-lipid clusters have been observed by Brewster angle microscopy (BAM) for much larger nanoparticles (107 nm) and at 10-fold higher nanoparticle-lipid ratio[21], to our knowledge, there has been no direct evidence that a condensed phase has been induced from an LE-forming lipid. BAM imaging yielded no evidence for such clusters in this system (data not shown) however the particle size is much smaller, and clusters may be below the 1 μm limit of resolution of BAM. For POPG, the critical temperature above which no monolayer condensed phase is observed has been reported to be 20 °C (i.e., below this temperature a condensed phase can be induced at high pressures).[49] Thus, it appears that the interaction of the cationic NPs with the anionic lipid head groups can sufficiently reduce the charge repulsion, resulting in a shift of the critical temperature by a few degrees such that a condensed phase can be formed. This condensation will affect the LE-C phase ratio. Alonso *et al.*[46] demonstrated that the viscosity of lung surfactant is highly sensitive to this ratio with a significant increase in viscosity beyond a critical condensed phase fraction. They noted that subtle changes in this ratio could have a significant impact on the mechanical properties of lung surfactant films.

Herein, we have shown that cationic NPs have a significantly greater impact on lung surfactant than anionic NPs. This is concordant with cytotoxicity studies that have shown that charged NPs have a more cytotoxic effect on non-phagocytic cell membranes than neutral forms,[60] with cationic particles being more cytotoxic than anionic ones.[61–65] Furthermore, computational modeling[66] and experimental studies[67] have shown that cationic NPs penetrate into lipid films containing anionic phosphatidylglycerols, while anionic particles do not penetrate either in DPPC, DSPC or DPPC:POPG membranes. It has been shown that the interaction with anionic NPs induces a film expansion, albeit in systems with much higher particle concentrations.[4,27] At the much lower concentrations used here, isotherm expansions are not always observed, even when significant structural changes are induced via lipid-NP interactions. Moreover, even at low concentrations, anionic particles can hinder the formation of condensed domains, as has been previously observed,[25,26] shifting the LE-C phase transition to higher surface pressures.

Conclusions

The structural organization of the condensed phase in lung surfactant films can be modified by exposure to low concentrations of charged silica nanoparticles. The choice of lipids to model the liquid-expanded and condensed phases of lung surfactant is an important parameter. First of all, the extent of lipid partial miscibility is a function of the choice of the fluid-phase forming lipid and this can cause subtle changes to the DPPC-rich condensed phase. The similarity of the structural changes for DPPC:POPG and Infasurf upon interaction with the NPs suggests that using a charged (anionic) lipid such as POPG as the fluid-phase forming lipid provides a better mimics of the natural extract Infasurf. For hydrophilic NPs dispersed in the subphase, anionic NPs interact with the lipid head groups, but only induce a small change in the lipid head group and alkyl chain organization and orientation as determined by GIXD and XR. These results are in agreement with previous studies on anionic NPs causing a slight expansion of the condensed phase.[4] While much attention has been given to negatively-charged particles (e.g., hydroxyapatite, polystyrene, engineered carbon nanodiamonds, and silica), at the low concentration of 0.001 wt%, it is the cationic NPs that have a marked effect on the structure of the film. In particular, the cationic NPs induce a condensation of the normally fluid phase POPG resulting in a large net reduction of the chain tilt angle in the condensed phase. This has implications for the LE-C phase ratio and consequently the film mechanical properties.

Conflicts of interest

There are no conflicts to declare.

Acknowledgements

AB and CD acknowledge funding from the FRQNT team research project program (2015-PR-183946). OB thanks the FRQNT for a postdoctoral research scholarship. MF thanks the Groupe de recherche en physique et technologie des couches minces for an Arthur Yelon-John Low Brebner summer scholarship. ChemMatCARS Sector 15 is principally supported

by the Divisions of Chemistry (CHE) and Materials Research (DMR), National Science Foundation, under grant number NSF/CHE-1346572. Use of the Advanced Photon Source, an Office of Science User Facility operated for the U.S. Department of Energy (DOE) Office of Science by Argonne National Laboratory, was supported by the U.S. DOE under Contract No. DE-AC02-06CH11357.

References

1 C. Stefaniu and G. Brezesinski, X-ray investigation of monolayers formed at the soft air/water interface, *Curr. Opin. Colloid Interface Sci.*, 2014, **19**, 216–227.

2 V. Kaganer, H. Möhwald and P. Dutta, Structure and phase transitions in Langmuir monolayers, *Rev. Mod. Phys.*, 1999, **71**, 779–819.

3 K. A. Dawson, A. Salvati and I. Lynch, Nanotoxicology: Nanoparticles reconstruct lipids, *Nat Nano*, 2009, **4**, 84–85.

4 A. Chakraborty, N. J. Mucci, M. L. Tan, A. Steckley, T. Zhang, M. L. Forrest and P. Dhar, Phospholipid composition modulates carbon nanodiamond-induced alterations in phospholipid domain formation, *Langmuir*, 2015, **31**, 5093–5104.

5 I. Theodorou, M. Ryan, T. Tetley and A. Porter, Inhalation of Silver Nanomaterials—Seeing the Risks, *Int. J. Mol. Sci.*, 2014, **15**, 23936–23974.

6 European Commission Health and Consumer Protection Directorate-General Scientific Committee on Consumer Products, *Preliminary opinion on safety of nanomaterials in cosmetic products*, Brussels, 2007.

7 M. Griese, Pulmonary surfactant in health and human lung diseases: state of the art., *Eur. Respir. J.*, 1999, **13**, 1455–76.

8 H. M. Mansour, Y. S. Rhee and X. Wu, Nanomedicine in pulmonary delivery., *Int. J. Nanomedicine*, 2009, **4**, 299–319.

9 S. Tatur and A. Badia, Influence of hydrophobic alkylated gold nanoparticles on the phase behavior of monolayers of DPPC and clinical lung surfactant, *Langmuir*, 2012, **28**, 628–639.

10 C. Mühlfeld, B. Rothen-Rutishauser, F. Blank, D. Vanhecke, M. Ochs and P. Gehr, Interactions of nanoparticles with pulmonary structures and cellular responses., *Am. J. Physiol. Lung Cell. Mol. Physiol.*, 2008, **294**, L817–L829.

11 A. A. Kapralov, W. H. Feng, A. A. Amoscato, N. Yanamala, K. Balasubramanian, D. E. Winnica, E. R. Kisin, G. P. Kotchey, P. Gou, L. J. Sparvero, P. Ray, R. K. Mallampalli, J. Klein-Seetharaman, B. Fadeel, A. Star, A. A. Shvedova and V. E. Kagan, Adsorption of surfactant lipids by single-walled carbon nanotubes in mouse lung upon pharyngeal aspiration, *ACS Nano*, 2012, **6**, 4147–4156.

12 K. Donaldson and C. A. Poland, *Swiss Med. Wkly.*, 2012, 142.

13 C. Schleh, C. Mühlfeld, K. Pulskamp, A. Schmiedl, M. Nassimi, H. D. Lauenstein, A. Braun, N. Krug, V. J. Erpenbeck and J. M. Hohlfeld, The effect of titanium dioxide nanoparticles on pulmonary surfactant function and ultrastructure., *Respir. Res.*, 2009, **10**, 90.

14 M. S. Bakshi, L. Zhao, R. Smith, F. Possmayer and N. O. Petersen, Metal nanoparticle pollutants interfere with pulmonary surfactant function in vitro., *Biophys. J.*, 2008, **94**, 855–68.

15 C. Schleh, C. Muhlfeld, K. Pulskamp, A. Schmiedl, A. Braun, M. Nassimi, H. D. Lauenstein, N. Krug, V. J. Erpenbeck and J. M. Hohlfeld, Titanium Dioxide Nanoparticles Alter Pulmonary Surfactant Ultrastructure and Biophysical Function., *Am. J. Respir. Crit. Care Med.*, 2009, **179**, A5255.

16 A. T. Kodama, C.-C. Kuo, T. Boatwright and M. Dennin, Investigating the Effect of Particle Size on Pulmonary Surfactant Phase Behavior, *Biophys. J.*, 2014, **107**, 1573–1581.

17 A. K. Sachan, R. K. Harishchandra, C. Bantz, M. Maskos, R. Reichelt and H. J. Galla, High-resolution investigation of nanoparticle interaction with a model pulmonary surfactant monolayer, *ACS Nano*, 2012, **6**, 1677–1687.

18 R. K. Harishchandra, M. Saleem and H.-J. Galla, Nanoparticle interaction with model lung surfactant monolayers, *J. R. Soc. Interface*, 2010, **7**, S15–S26.

19 A. K. Sachan and H. J. Galla, Understanding the mutual impact of interaction between hydrophobic nanoparticles and pulmonary surfactant monolayer, *Small*, 2014, **10**, 1069–1075.

20 M. V. Dwivedi, R. K. Harishchandra, O. Koshkina, M. Maskos and H. J. Galla, Size influences the effect of hydrophobic nanoparticles on lung surfactant model systems, *Biophys. J.*, 2014, **106**, 289–298.

21 W. Daear, P. Lai, M. Anikovskiy and E. J. Prenner, Differential Interactions of Gelatin Nanoparticles with the Major Lipids of Model Lung Surfactant: Changes in the Lateral Membrane Organization, *J. Phys. Chem. B*, 2015, **119**, 5356–5366.

22 A. Nel, T. Xia, L. Mädler and N. Li, Toxic potential of materials at the nanolevel., *Science*, 2006, **311**, 622–627.

23 G. Hu, B. Jiao, X. Shi, R. P. Valle, Q. Fan and Y. Y. Zuo, Physicochemical Properties of Nanoparticles Regulate Translocation across Pulmonary Surfactant Monolayer and Formation of Lipoprotein Corona, *ACS Nano*, 2013, **7**, 10525–10533.

24 Q. Fan, Y. E. Wang, X. Zhao, J. S. C. Loo and Y. Y. Zuo, Adverse biophysical effects of hydroxyapatite nanoparticles on natural pulmonary surfactant, *ACS Nano*, 2011, **5**, 6410–6416.

25 E. Guzmán, L. Liggieri, E. Santini, M. Ferrari and F. Ravera, DPPC-DOPC Langmuir monolayers modified by hydrophilic silica nanoparticles: Phase behaviour, structure and rheology, *Colloids Surf. A*, 2012, **413**, 174–183.

26 E. Guzmán, L. Liggieri, E. Santini, M. Ferrari and F. Ravera, Mixed DPPC-cholesterol Langmuir monolayers in presence of hydrophilic silica nanoparticles, *Colloids Surfac. B*, 2013, **105**, 284–293.

27 E. Guzmán, L. Liggieri, E. Santini, M. Ferrari and F. Ravera, Influence of silica nanoparticles on phase behavior and structural properties of DPPC-Palmitic acid Langmuir monolayers, *Colloids Surfac. A*, 2012, **413**, 280–287.

28 A. M. Farnoud and J. Fiegel, Low concentrations of negatively charged sub-micron particles alter the microstructure of DPPC at the air–water interface, *Colloids Surfac. A*, 2012, **415**, 320–327.

29 H. Zhang, Q. Fan, Y. E. Wang, C. R. Neal and Y. Y. Zuo, Comparative study of clinical pulmonary surfactants using atomic force microscopy., *Biochim. Biophys. Acta*, 2011, **1808**, 1832–42, and references therein.

30 B. R. Bzdek, A. J. Horan, M. R. Pennington, N. J. Janechek, J. Baek, C. O. Stanier and M. V. Johnston, Silicon is a frequent component of atmospheric nanoparticles, *Environ. Sci. Technol.*, 2014, **48**, 11137–11145.

31 C. M. Sayes, K. L. Reed and D. B. Warheit, Assessing toxicology of fine and nanoparticles: Comparing in vitro measurements to in vivo pulmonary toxicity profiles, *Toxicol. Sci.*, 2007, **97**, 163–180.

32 D. Rees and J. Murray, *Int. J. Tuberc. Lung Dis.*, 2007, 11, 474–484.

33 G. Brezesinski, A. Dietrich, B. Struth, C. Böhm, W. G. Bouwman, K. Kjaer and H. Möhwald, Influence of ether linkages on the structure of double-chain phospholipid monolayers, *Chem. Phys. Lipids*, 1995, **76**, 145–157.

34 F. Bringezu, J. Ding, G. Brezesinski and J. A. Zasadzinski, Changes in model lung surfactant monolayers induced by palmitic acid, *Langmuir*, 2001, **17**, 4641–4648.
35 J. R. Silvius, Thermotropic Phase Transition of Pure Lipids in Model Membranes and Their Modifications by Membrane Proteins. In *Lipid-Protein Interactions*, John Wiley & Sons, Inc., New York, 1982.
36 J. Ding, I. Doudevski, H. E. Warriner, T. Alig, J. A. Zasadzinski, A. J. Waring and M. A. Sherman, Nanostructure Changes in Lung Surfactant Monolayers Induced by Interactions between Palmitoyloleoylphosphatidylglycerol and Surfactant Protein B, *Langmuir*, 2003, **19**, 1539–1550.
37 A. Guinier, *X-ray Diffraction in Crystals, Imperfect Crystals and Amorphous Bodies*, W. H. Freeman and Co, San Francisco, London, 1968.
38 K. Kjaer, Some simple ideas on X-ray reflection and grazing-incidence diffraction from thin surfactant films, *Phys. B Phys. Condens. Matter*, 1994, **198**, 100–109.
39 W. Bu, M. Mihaylov, D. Amoanu, B. Lin, M. Meron, I. Kuzmenko, L. Soderholm and M. L. Schlossman, X-ray studies of interfacial strontium-extractant complexes in a model solvent extraction system, *J. Phys. Chem. B*, 2014, **118**, 12486–12500.
40 S. S. You, C. T. R. Heffern, Y. Dai, M. Meron, J. M. Henderson, W. Bu, W. Xie, K. Y. C. Lee and B. Lin, Liquid Surface X-ray Studies of Gold Nanoparticle-Phospholipid Films at the Air/Water Interface, *J. Phys. Chem. B*, 2016, **120**, 9132–9141.
41 L. G. Parratt, Surface Studies of Solids, *Phys. Rev.*, 1954, **95**, 359–369.
42 Y. Dai, B. Lin, M. Meron, K. Kim, B. Leahy, T. A. Witten and O. G. Shpyrko, Synchrotron X-ray studies of rapidly evolving morphology of self-assembled nanoparticle films under lateral compression, *Langmuir*, 2013, **29**, 14050–14056.
43 Y. Dai, B. Lin, M. Meron, K. Kim, B. Leahy and O. G. Shpyrko, A Comparative Study of Langmuir Surfactant Films: Grazing Incidence X-Ray off-Specular Scattering vs. X-Ray Specular Reflectivity, *J. Appl. Phys.*, **2011**, 110, 102213-102213-6.
44 P. C. Stenger, G. Wu, C. E. Miller, E. Y. Chi, S. L. Frey, K. Y. C. Lee, J. Majewski, K. Kjaer and J. A. Zasadzinski, X-ray diffraction and reflectivity validation of the depletion attraction in the competitive adsorption of lung surfactant and albumin, *Biophys. J.*, 2009, **97**, 777–786.
45 K. Y. C. Lee, J. Majewski, T. L. Kuhl, P. B. Howes, K. Kjaer, M. M. Lipp, A. J. Waring, J. A. Zasadzinski and G. S. Smith, Synchrotron X-Ray Study of Lung Surfactant-Specific Protein SP-B in Lipid Monolayers, *Biophys. J.*, 2001, **81**, 572–585.
46 C. Alonso, A. Waring and J. A. Zasadzinski, Keeping lung surfactant where it belongs: Protein regulation of two-dimensional viscosity, *Biophys. J.*, 2005, **89**, 266–273.
47 A. Mangiarotti, B. Caruso and N. Wilke, Phase coexistence in films composed of DLPC and DPPC: A comparison between different model membrane systems, *Biochim. Biophys. Acta - Biomembr.*, 2014, **1838**, 1823–1831.
48 J. Sanchez and A. Badia, Spatial variation in the molecular tilt orientational order within the solid domains of phase-separated, mixed dialkylphosphatidylcholine monolayers, *Chem. Phys. Lipids*, 2008, **152**, 24–37.
49 D. Y. Takamoto, M. M. Lipp, a von Nahmen, K. Y. Lee, a J. Waring and J. a Zasadzinski, Interaction of lung surfactant proteins with anionic phospholipids., *Biophys. J.*, 2001, **81**, 153–169.
50 S. L. Selladurai, R. Miclette Lamarche, R. Schmidt and C. E. Dewolf, Model Lung Surfactant Films: Why Composition Matters, *Langmuir*, 2016, **32**, 10767–10775.
51 M. M. Lipp, K. Y. C. Lee, J. A. Zasadzinski and A. J. Waring, Design and performance of an integrated fluorescence, polarized fluorescence, and Brewster angle microscope/Langmuir trough assembly for the study of lung surfactant monolayers, *Rev. Sci. Instrum.*, 1997, **68**, 2574–2582.
52 J. Sanchez and A. Badia, Atomic force microscopy studies of lateral phase separation in mixed monolayers of dipalmitoylphosphatidylcholine and dilauroylphosphatidylcholine, *Thin Solid Films*, 2003, **440**, 223–239.
53 R. B. Gennis, The Structures and Properties of Membrane Lipids. In *Biomembranes: Molecular Structure and Function*, ed. R. B. Gennis, Springer New York: New York, NY, 1989; pp 36–84.
54 A. Badia, P. Moraille, N. Y. W. Tang and M. E. Randlett, Nanostructured phospholipid membranes, *Int. J. Nanotechnol.*, 2008, **5**, 1371–1395.
55 C. Alonso, F. Bringezu, G. Brezesinski, A. J. Waring and J. A. Zasadzinski, Modifying calf lung surfactant by hexadecanol, *Langmuir*, 2005, **21**, 1028–1035.
56 P. G. Scherer and J. Seelig, Electric Charge Effects on Phospholipid Headgroups. Phosphatidylcholine in Mixtures with Cationic and Anionic Amphiphilest, *Biochemistry*, 1989, **28**, 7720–7728.
57 L. Saiz and M. L. Klein, Electrostatic interactions in a neutral model phospholipid bilayer by molecular dynamics simulations, *J. Chem. Phys.*, 2002, **116**, 3052–3057.
58 M. Christoforou, E. Leontidis and G. Brezesinski, Effects of sodium salts of lyotropic anions on low-temperature, ordered lipid monolayers, *J. Phys. Chem. B*, 2012, **116**, 14602–14612.
59 A. Hädicke and A. Blume, Binding of the Cationic Peptide (KL)4K to Lipid Monolayers at the Air–Water Interface: Effect of Lipid Headgroup Charge, Acyl Chain Length, and Acyl Chain Saturation, *J. Phys. Chem. B*, 2016, **120**, 3880–3887.
60 N. M. Schaeublin, L. K. Braydich-Stolle, A. M. Schrand, J. M. Miller, J. Hutchison, J. J. Schlager and S. M. Hussain, Surface charge of gold nanoparticles mediates mechanism of toxicity, *Nanoscale*, 2011, **3**, 410.
61 M. Baek, I.-S. Kim, J. Yu, H. E. Chung, J.-H. Choy and S.-J. Choi, Effect of different forms of anionic nanoclays on cytotoxicity., *J. Nanosci. Nanotechnol.*, 2011, **11**, 1803–6.
62 S. Bhattacharjee, L. H. J. De Haan, N. M. Evers, X. Jiang, A. T. M. Marcelis, H. Zuilhof, I. M. C. M. Rietjens and G. M. Alink, Role of surface charge and oxidative stress in cytotoxicity of organic monolayer-coated silicon nanoparticles towards macrophage NR8383 cells, *Part. Fibre Toxicol.*, 2010, 25.
63 C. M. Goodman, C. D. McCusker, T. Yilmaz and V. M. Rotello, Toxicity of gold nanoparticles functionalized with cationic and anionic side chains, *Bioconjug. Chem.*, 2004, **15**, 897–900.
64 W. K. Oh, S. Kim, M. Choi, C. Kim, Y. S. Jeong, B. R. Cho, J. S. Hahn and J. Jang, Cellular uptake, cytotoxicity, and innate immune response of silica-Titania hollow nanoparticles based on size and surface functionality, *ACS Nano*, 2010, **4**, 5301–5313.
65 L. Ruizendaal, S. Bhattacharjee, K. Pournazari, M. Rosso-Vasic, L. H. J. De Haan, G. M. Alink, A. T. M. Marcelis and H. Zuilhof, Synthesis and cytotoxicity of silicon nanoparticles with covalently attached organic monolayers, *Nanotoxicology*, 2009, **3**, 339–347.
66 J. Lin, H. Zhang, Z. Chen and Y. Zheng, Penetration of lipid membranes by gold nanoparticles: Insights into cellular uptake, cytotoxicity, and their relationship, *ACS Nano*, 2010, **4**, 5421–5429.
67 S. Tatur, M. MacCarini, R. Barker, A. Nelson and G. Fragneto, Effect of functionalized gold nanoparticles on floating lipid bilayers, *Langmuir*, 2013, **29**, 6606–6614.

Environmental Science: Nano

ARTICLE

Table 1. Height differences and percent area coverages determined for DPPC:DLPC, DPPC:POPG, and Infasurf.

Lipid System	Height difference (LE-C) [Å][a]	% area coverage of condensed phase[a]
DPPC:DLPC (7:3)	5.8 ± 0.8	48 ± 14
DPPC:POPG (7:3)	5.2 ± 0.6	65 ± 7
Infasurf	5.6 ± 0.4	40 ± 8

[a] Height differences and percent area coverages determined from an analysis of the depth histograms of 2-4 AFM images acquired on different areas of the sample.

Table 2. d spacings, chain tilt (t), projected area per chain (A_{xy}), lattice type, and tilt azimuth for DPPC, DPPC:DLPC (7:3), and DPPC:POPG (7:3) on subphases of water, 0.001 wt% anionic NPs, and 0.001 wt% cationic NPs, calculated from GIXD measurements at 35 mN/m and 22.0 ± 0.5 °C.

System	Subphase	d (10) [Å]	d (01) [Å]	d (1±1) [Å]	Chain tilt[a] [°]	A_{xy}[a] [Å^2]	Lattice	Tilt azimuth
DPPC	Water	4.60	4.47	4.28	27.1	22.9	Oblique	Intermediate
DPPC	Anionic NPs	4.74	4.65	4.29	32.7	24.1	Oblique	Intermediate
DPPC	Cationic NPs	4.71	4.60	4.29	31.3	23.3	Oblique	Intermediate
DPPC:DLPC	Water	4.65	4.59	4.29	28.4	23.5	Oblique	Intermediate
DPPC:DLPC	Anionic NPs	4.62	4.46	4.28	26.7	23.0	Oblique	Intermediate
DPPC:DLPC	Cationic NPs	4.72	4.63	4.29	28.4	23.9	Oblique	Intermediate
DPPC:POPG	Water	4.46	4.38	4.26	20.0	22.0	Oblique	Intermediate
DPPC:POPG	Anionic NPs	4.50	4.43	4.28	22.7	22.4	Oblique	Intermediate
DPPC:POPG	Cationic NPs	4.26	4.35	4.26	6.8	21.5	Centered rectangular	NNN

[a] The chain tilt (t) is the angle of the fully-extended alkyl chain relative to the normal and A_{xy} is the area occupied by the chain in the x-y plane.

Table 3. Fitted parameters for XR data for DPPC, DPPC:DLPC (7:3), and DPPC:POPG (7:3) on subphases of water, 0.001 wt% anionic NPs, and 0.001 wt% cationic NPs at 35 mN/m and 22 ± 0.5 °C.

System	Subphase	Tail		Head group		Nanoparticle		
		Thickness [Å]	ρ [e^-/Å^3]	Thickness [Å]	ρ [e^-/Å^3]	Thickness [Å]	ρ [e^-/Å^3]	σ[a] [Å]
DPPC	Water	15.9	0.317	8.7	0.455	--	--	3.47
DPPC	Anionic NPs	15.8	0.321	7.9	0.470	160.4	0.334	3.31
DPPC	Cationic NPs	15.4	0.314	9.2	0.453	227.7	0.334	3.46
DPPC:DLPC	Water	13.3	0.324	8.7	0.418	--	--	3.62
DPPC:DLPC	Anionic NPs	13.6	0.323	8.0	0.417	150.5	0.335	3.68
DPPC:DLPC	Cationic NPs	12.9	0.320	9.3	0.413	228.3	0.335	3.62
DPPC:POPG	Water	17.5	0.320	8.5	0.463	--	--	3.79
DPPC:POPG	Anionic NPs	17.2	0.326	7.9	0.477	159.7	0.334	3.87
DPPC:POPG	Cationic NPs	15.5	0.312	10.6	0.476	223.4	0.339	4.02

[a] σ is the root mean square of roughness at the interface.

Table of Contents Entry

Nanoparticle-Induced Structural Changes in Lung Surfactant Membranes: An X-ray Scattering Study

Shirin Behyan,[a,b] Olga Borozenko,[a,b] Abdullah Khan,[a] Manon Faral,[b] Antonella Badia,*[b,c] and Christine DeWolf*[a,c]

[a]Department of Chemistry and Biochemistry and Centre for NanoScience Research, Concordia University, 7141 Sherbrooke St. West, Montréal, QC H4B 1R6, Canada. E-mail: christine.dewolf@concordia.ca

[b]Address here. Département de chimie, Université de Montréal, C.P. 6128 succursale Centre-ville, Montréal, QC H3C 3J7, Canada. E-mail: antonella.badia@umontreal.ca

[c]FRQNT Quebec Centre for Advanced Materials.

*Corresponding Authors Contact Information:

E-mail: christine.dewolf@concordia.ca

E-mail: antonella.badia@umontreal.ca

Low concentrations of cationic silica nanoparticles impact lung surfactant membrane structure while anionic nanoparticles have minimal effect.